On the role of water, temperature, and glass transition in the corrosion protection behavior of epoxy coatings for underground pipelines

Hung M. Ha, Akram Alfantazi

Abstract Water transport kinetics in the coatings were markedly enhanced and the coating impedances decreased exponentially as temperature increased. The effect of temperature on the coating impedance was attributed to the change in the defect area fraction caused by the thermal expansion of the polymers. The temperature dependence of coating impedance was reversible in a non-aqueous environment but was irreversible in an aqueous environment. This is attributed to the plasticization effect of water on the polymer chains. The effect of glass transition on coating impedances during a short period of exposure to heat source was insignificant.

Keywords Polymer coatings, Degradation, Glass transition, Corrosion, High temperature

Introduction

Pipeline segments near compression stations are exposed to high-temperature gases whose temperature may rise to 70°C and above if proper cooling systems are not installed. Polymer coatings on such pipeline segments may experience glass transition. Thermodynamically, the glass transition is a second-order transition in which there is no discontinuity in the Gibbs free energy and its first partial derivatives such as the entropy, volume, or enthalpy at the glass transition temperature (T_g), but there is discontinuity in the second partial derivatives of the Gibbs free energy such as the heat capacitance, compressibility, and dielectric constant.[1,2] On the molecular scale, the glass transition involves the onset of long-range coordinated molecular motion, the beginning of reptation.[2] On the macroscopic scale, the mechanical properties, thermal properties, and electrical properties of the polymers[2–4] abruptly change in the glass transition range. These changes may have profound effects on the corrosion protection performance of polymer coatings working above T_g.

The adverse effects of temperature on the corrosion protection performance of polymer coatings have been reported in the literature;[5–13] however, the effect of temperature above T_g was only reported in a few studies.[8,11,12,14] One of the studies revealed that the low-frequency impedance of a polymer coating which corresponds to the resistance of the coating to ionic transport sharply decreased at the glass transition temperature ($T_g = 35°C$) and was approximately two orders of magnitude smaller at 75°C compared to the same coating at 25°C.[8] Another study reported that both coating impedance at 1 Hz and storage modulus obtained from dynamic mechanical thermal analysis (DMTA) experienced a sharp decrease as temperatures exceeded T_g.[14] The sharp decrease of the low-frequency impedance indicates a significant increase in the ionic conductivity of the coating above T_g which facilitates the formation of conductive pathways in the first stage of coating failure. It is likely that the adverse effect of temperature is particularly significant above T_g.

Electrochemical impedance spectroscopy (EIS) has been extensively used to predict the long-term performance of polymer coatings on metal substrates.[15–22] The coating impedance was used as an indication of the quality of the coatings.[16–18,22] The change in the coating capacitance was related to the amount of water uptake by the coatings.[23,24] In addition, the phase shift in the EIS data was used to quantify the delaminated areas at the coating-substrate interface utilizing the breakpoint frequency value.[15,18,19] However, there is controversy over the sensitivity of this breakpoint frequency method

H. M. Ha (✉), A. Alfantazi
Corrosion Group, Department of Materials Engineering, The University of British Columbia, Vancouver, BC V6T1Z4, Canada
e-mail: hungha@mail.ubc.ca

to the delaminated areas associated with blister.[25–28] Recently, EIS was used to study the transport of water in coatings by monitoring the rise and decay of the coating capacitance as the electrolyte is switched between aqueous medium and hydrophilic room temperature ionic liquids (RTIL).[29–31] The use of RTIL as a conducting medium in EIS measurement gives opportunities to isolate the effect of water on polymer from other factors such as temperature.

This study investigated the effect of water absorption, temperature, and glass transition on the performance of high-temperature coatings for oil and gas transmission pipelines. RTIL was used as the conducting media for EIS experiments to isolate the impacts of water plasticization[29–31] that might complicate the interpretation of the data. Changes in the corrosion protection properties of the coatings were interpreted in terms of structural and compositional changes of the polymers as well as the changes in the transport kinetics of electrolyte through the coatings. A link between temperature, polymer structure, and coatings performance was established.

Experiment

Materials and electrolytes

Bisphenol A and Novolac coatings provided by Specialty Polymer Coatings Inc. were used in this study. Carbon steel substrates (0.2C 0.76Mn 0.2Si 0.03S 0.01P 0.04Mo 0.37Cu 0.11Ni 0.11Cr 0.001Ti and Fe-balanced, in wt%) were abrasively blasted to achieve a surface roughness between 62.5 and 125 μm. Coatings of 500 ± 50 μm thick on carbon steel substrates were performed by spray coating. The coatings were then cured at 40°C for 3 days in a hot-air oven and then kept at 25°C in air for 15 days. Substrate-free polymer films of 500 ± 50 μm thick were prepared by spraying the coatings on a glass plate and the plate was removed after the coatings had been cured.

Room temperature ionic liquid (1-butyl-1-methylpyrrolidinium trifluoromethanesulfonate) and 3 wt% NaCl solution were used as the electrolytes in electrochemical tests. The conductivity of the RTIL changes from 0.002 to 0.006 S cm^{-1} when temperature increases from 20 to 80°C,[29] which is about one-tenth of the conductivity of the 3 wt% NaCl solution at the same temperature. The ionic liquid was acquired from EDM Milipore Chemicals. The 3 wt% NaCl solution was prepared from reagent grade NaCl with deionized water.

Differential scanning calorimetry (DSC)

The glass transition temperatures of the polymers before and after soaking in water were determined using a TA Instrument Q1000 differential scanning calorimeter (DSC). DSC experiments were performed on coatings that were dry, 3-day water-soaked at 20°C, and 3-day water-soaked at 80°C. The heat flow was recorded when the temperature was increased from 25 to 150°C at 4°C/min. T_g was determined from the sigmoidal step change in the reverse heat capacity signal following ASTM E2602.[32] Three DSC experiments for each material were performed and average values were reported.

Fourier transform infrared spectroscopy (FTIR)

The effect of temperature and water absorption on the chemistry of the polymers was examined using an attenuated total reflectance (ATR)-FTIR (Agilent Cary 660 FTIR) equipped with a temperature-controlled, hot stage attachment. Freshly prepared samples and samples soaked in water at 80°C for 20 days were characterized. The samples were heated at a rate of 4°C/min and the measurement was performed at every 10°C increment. The spectrum was scanned from 500 to 4000 cm^{-1}.

Water uptake

The water uptake was determined by the gravimetric method.[33] The weight gain of the substrate-free coating sheets during immersion in 3 wt% NaCl solution at 20 and 80°C was measured by a Sciencetech ZSA120 analytical scale with an accuracy of 0.1 mg. The water transport in the polymer coatings was assumed to follow Fick's laws of diffusion. The water uptake by diffusion in a plane sheet of uniform material immersed in a solution is expressed by the following[34]:

$$\frac{M_t}{M_\infty} = 1 - \frac{8}{\pi^2} \sum_{m=0}^{\infty} \frac{1}{(2m+1)^2} \exp\left\{ -D(2m+1)^2 \pi^2 t / l^2 \right\},$$

(1)

where M_t is the total amount of water absorbed by the sheet at time t (g), M_∞ is the equilibrium sorption level attained theoretically after infinite time (g), D is the water diffusivity in the polymer (cm^2/s), l is the thickness of the polymer sheet (cm), and t is the immersion time (s). The following equation was used to determine the water diffusivity in the coatings when the time to half-saturation, $t_{0.5}$, is measured[34]:

$$D = 0.049 \cdot \frac{l^2}{t_{0.5}}.$$

(2)

Electrochemical impedance spectroscopy (EIS)

A two-electrode double cell was used to perform EIS experiments on the substrate-free coating films at

different temperatures between 20 and 80°C (Fig. 1a). The substrate-free coating sample was sandwiched between the two identical cylindrical cells filled with test solution. The sample exposed an area of 38 cm^2 to the test solutions on both sides and separated the solutions in the two cell compartments. A platinized Ti mesh acting as either a working electrode or a counter electrode was used in each compartment. The test solutions and the coating samples were heated by hot water running inside glass coils.

Three-electrode cylindrical cells were used to perform EIS experiments on the coated steel samples at temperatures between 20 and 80°C (Fig. 1b). The cells were constructed by attaching plexiglas cylinders to the coating surface. The exposed area of the coatings was 32 cm^2. The cell also included a high-temperature silver–silver chloride reference electrode and a platinized Ti mesh counter electrode. The whole setup was heated to the desired temperatures using an oven.

The coated samples and substrate-free coatings were allowed to stabilize at the desired temperature for approximately 1 h before commencing electrochemical measurements. Then the temperature was increased and the same procedure was repeated. When the temperature reached 80°C, the samples were cooled down overnight in air to ambient temperature before

the next heating and electrochemical measurement cycle started. EIS experiments were performed at the open circuit potentials (OCP) with an alternative potential perturbation of 100 mV and a frequency scan from 100 kHz to 10 mHz using a Gamry Reference 600 potentiostat. The OCPs of the coated steel samples before EIS measurements decreased from ca. −400 to −600 mV vs saturated calomel electrode (SCE) as the temperature increased from 20 to 80°C and did not change more than 20 mV over the period of 15 min.

EIS data analysis

EIS data of substrate-free coatings were analyzed using the equivalent electrical circuit in Fig. 2a. In this model, R_s was the solution resistance which was negligible for the particular experiment setup in this study. A constant phase element CPE$_c$ was used to represent the non-idea capacitance response of the coating. The resistance to the transport of water and ionic species from the solution to the steel substrate via defects and pores in the coatings was represented by a pore resistance R_p. The equivalent circuit in Fig. 2b is commonly used to analyze EIS data of coated steel systems.[16–19,21,22,27,28,35–39] In addition to the components representing the electrolyte and the coating, a constant phase element of the double-layer CPE$_{dl}$ in parallel with a charge transfer resistance R_{ct} are in series with R_p to account for the corrosion of the steel substrate at the bottom of the defects and pores. The
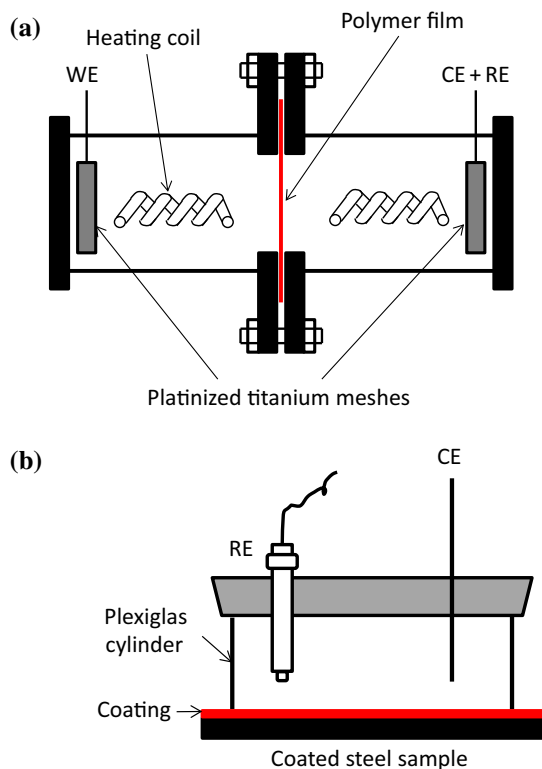

Fig. 1: Schematic of the EIS experiment setup. (a) Double-cell setup for EIS measurement of substrate-free coating films. (b) Three-electrode configuration setup for EIS measurement of coated steel samples. *WE* working electrode, *RE* reference electrode, *CE* counter electrode
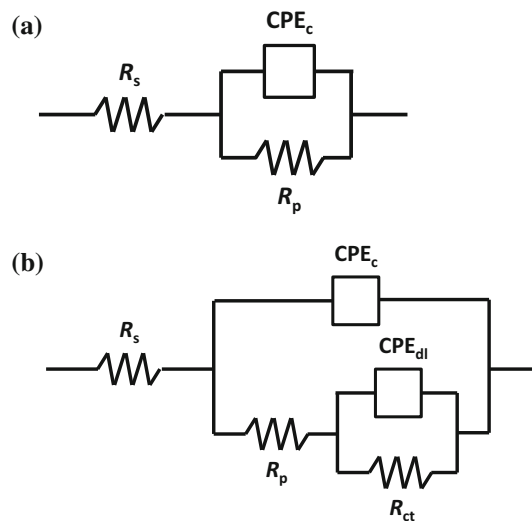

Fig. 2: Equivalent electrical circuit representing (a) a substrate-free coating in the double-cell experiment and (b) a coated steel immersed in a solution. R_s-solution resistance, R_p-pore resistance of the coating, R_{ct}-charge transfer resistance of the corrosion reaction of the steel substrate, CPE$_c$-constant phase element of the coating, and CPE$_{dl}$-constant phase element of the double layer at the steel surface

pore resistance, charge transfer resistance, and the double-layer capacitance are related to the defect area fraction as expressed by equations (3) to (5)[16,17,19]:

$$R_p = \frac{1}{\kappa} \frac{\zeta d}{A_p}, \tag{3}$$

$$R_{ct} = r_{ct} \cdot A_p, \tag{4}$$

$$C_{dl} = \frac{c_{dl}}{A_p}, \tag{5}$$

where A_p is the pore area fraction, κ is the pore conductivity (S-cm^{-1}), ζ is the tortuosity factor of the pore in the coating, d is the coating thickness (cm), and R_{ct} and C_{dl} are the area-specific charge transfer resistance (Ω-cm^2) and the area-specific double-layer capacitance (F/cm^2) associated with the corrosion of the substrate.

Figures 3a and 3b show the simulated EIS data in the Bode plot of a substrate-free coating assuming different defect percentages. The capacitance of the coating was calculated for a 0.5-mm-thick and 38 cm^2 coating film with a relative permittivity of the polymer of 4. The conductivity of the solution inside the pores of the coatings was assumed to be 0.04 S/cm which was the conductivity of 3 wt% NaCl solution. The defect area in the coating was varied from 10^{-5} to 10^{-10}%. A linear relationship between log Z and log f with a slope of 45° was observed at the high-frequency range from 1 kHz to 1 MHz in Fig. 3a at all defect percentages. In this linear region, the measured image impedance, Z'', was related to the frequency, f, and the coating capacitance by

$$Z'' = \frac{1}{2\pi f C_c}. \tag{6}$$

In contrast, a plateau was observed at the low-frequency range in the impedance vs frequency plot (Fig. 3a). This impedance plateau was equal to the sum of R_s and R_p and decreased when the defect percentage increased. This impedance decrease was related to the decrease of R_p, as more defects are present in the coating. Therefore, monitoring the change in the impedance plateau allowed a direct determination of the change in the pore area fraction in coatings according to equation (3).

The break point at high-frequency f_h where the phase angle was equal to 45° (Fig. 3b) was used in many studies to quantify the defect area in coatings.[15–19,25–27] At this frequency, the contribution of the pore resistance and the coating capacitance to the overall impedance were equal, and therefore, the following relationship was derived[15,17,19,25]:

$$f_h = \frac{1}{2\pi\varepsilon_o} \frac{\kappa A_p}{\varepsilon \zeta}, \tag{7}$$
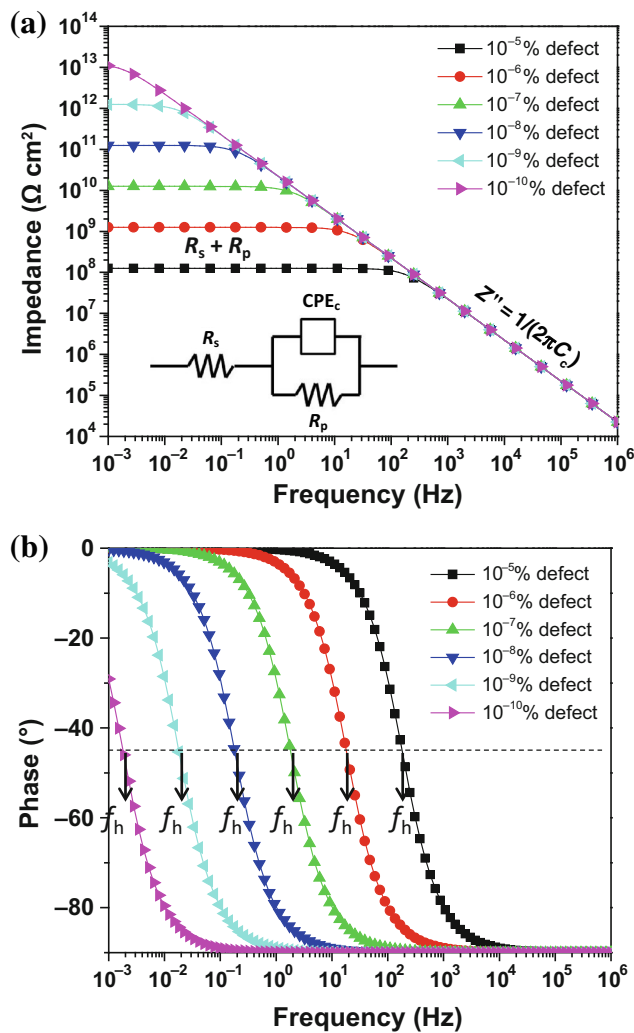

Fig. 3: EIS simulation results of the electrical equivalent circuit in Fig. 2a assuming different defect percentages in the coating. The total coating area was 38 cm^2, the coating thickness was 0.5 mm, the permittivity of the coating was 4, and the conductivity of the solution in the pores was 0.04 S cm^{-1}

where ε_o was the permittivity of vacuum ($\varepsilon_o = 8.8542 \times 10^{-14}$ F cm^{-1}) and ε was the relative permittivity of the coating. When κ and ε were constant, the change of f_h was directly related to the change in the tortuosity factor and the pore area fraction in the coating. However, in this study, it was likely that κ and ε would change as the temperature changed. Therefore, quantitative analysis using f_h was difficult.

Results

Determination of T_g

The results of DSC measurements on bisphenol A and Novolac coatings showing the dependence of the

reversing heat capacity (C_p) on temperature are presented in Fig. 4. In both coatings before and after water soaking (Figs. 4a and 4b), C_p increased as the temperature increased. Sigmoidal step increases in C_p indicating the glass transition event[32] were observed in all spectra. For instance, the sigmoidal step increase was observed between 40 and 60°C in the bisphenol A coating before soaking (Fig. 4a). Similarly, the sigmoidal step increase was observed between 70 and 90°C in the Novolac coating before soaking (Fig. 4a). The glass transition temperatures of the bisphenol A

(a)

Bisphenol A
Scan rate = 4°C/min

Soaked at 80°C

Soaked at 20°C

$T_g = 56 \pm 1$°C

Before soaking

$T_g = 42 \pm 1$°C

$T_g = 52 \pm 1$°C

(b)

Novolac
Scan rate = 4°C/min

Soaked at 80°C

Soaked at 20°C

$T_g = 80 \pm 1$°C

Before soaking

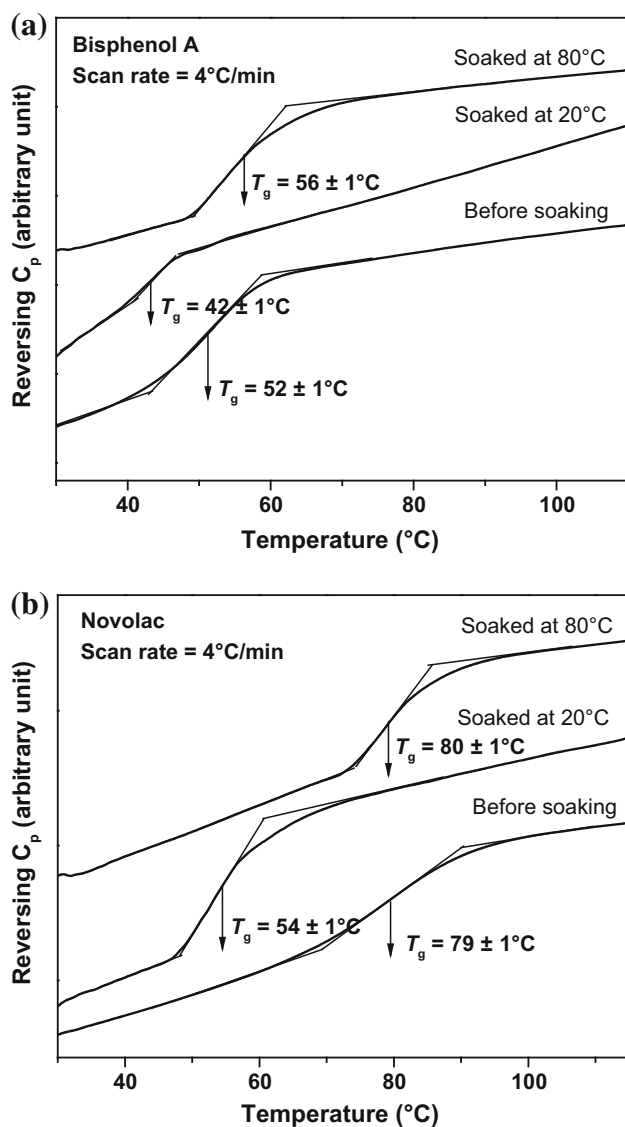$T_g = 54 \pm 1$°C

$T_g = 79 \pm 1$°C

Fig. 4: Dependence of the reversing heat capacity of bisphenol A and Novolac coatings on temperature. The tests were performed on dry coating powders and coating powders after soaking in water for 3 days at 20 and 80°C. The glass transition temperatures were determined from the sigmoidal step in the plot following ASTM E2602.[32] ± is the standard deviation of measured T_g obtained from 3 measurements

and the Novolac coatings before soaking were determined to be 52 ± 1 and 79 ± 1°C, respectively, using ASTM 2602 standard.[32] After soaking in water for 3 days at 20°C, the glass transition temperature of bisphenol A and Novolac coatings decreased to 42 ± 1 and 54 ± 1°C, respectively. The decrease in T_g of the bisphenol A coating could be attributed to the plasticization effect of water in the polymer which increased the mobility of the polymer segments. This behavior is well known in many polymer systems[40–42] and has been modeled by Kelley and Beuche[43] and extended by Zhou and Lucas.[44,45] After soaking in water for 3 days at 80°C, the glass transition temperature of bisphenol A and Novolac coatings increased to 56 ± 1 and 80 ± 1°C, respectively. The increase in T_g as the soaked temperature increased could be partially attributed to the effect of high activation energy bound waters which form a secondary crosslink network and therefore reduce the polymer chain mobility.[44,45]

Water absorption, desorption, and transport

Weight gains due to water absorption in bisphenol A and Novolac coatings during immersion in water at 20°C for 6 months and at 80°C for 9 days are plotted in Fig. 5. The amount of absorbed water in the coatings increased with time and gradually approached a plateau, indicating water saturation of the polymers (Fig. 5). After a 6-month immersion at 20°C, both bisphenol A and Novolac coatings gained ca. 3% and ca. 1.7% in weight, respectively (Fig. 5a). In contrast, at 80°C, both coatings quickly reached the level of saturation (i.e., ca. 3% for coating A and ca. 1.7% for coating B) in less than 4 h (Fig. 5b). After that the coatings continued absorbing more water but at a much slower rate. After baking the samples at 80°C in an oven for 7 days, the weights of all samples were reversed to the initial values prior to immersion, indicating all absorbed water was removed.

Water diffusivities in the coatings at 20 and 80°C were determined from the weight gain experiments. Assuming the driving force for water molecules penetrating the coatings was mainly due to concentration gradient, the rate of water transport in the polymer structure could be determined using equation (2). Figure 6b shows the water uptake fraction as a function of $t^{1/2}$. The data are not significantly deviated from the theoretical diffusion curves for different water diffusivities. This indicates a single-diffusion process dominated the water transport through the coatings. It should be noted that two or more diffusion processes were reported in other coating systems.[46,47] The time for the coatings to reach 50% saturation was determined from this plot. Using equation (2), the water diffusivities in the bisphenol A coating and the Novolac coating at 20°C were determined to be 2.7×10^{-10} and 4.1×10^{-10} cm^2/s, respectively. The water diffusivities in the bisphenol A coating and the Novolac coating at 80°C increased 2 orders of magni-
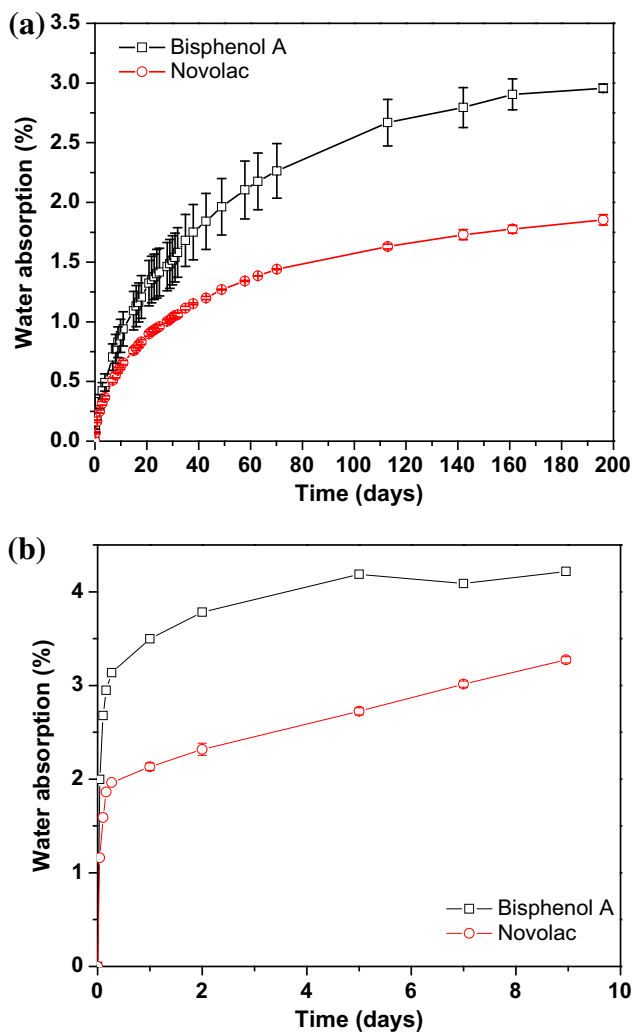
Fig. 5: Water absorption percentage of bisphenol A and Novolac coatings during immersion in water for (a) 6 months at 20°C and (b) 9 days at 80°C
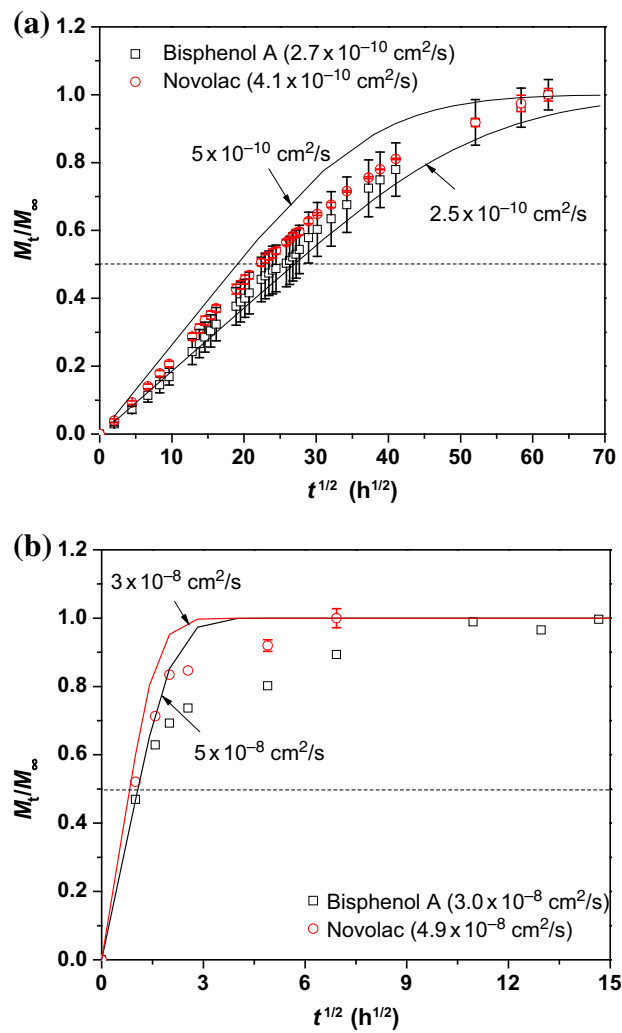

Fig. 6: Water uptake fraction of bisphenol A and Novolac coatings during immersion in water for (a) 6 months at 20°C and (b) 9 days at 80°C. Experiment data were plotted in open symbols and theoretical curves assuming different water diffusivities were plotted in solid lines

tude to 3.0×10^{-8} and 4.9×10^{-8} cm^2/s, respectively. The theoretical water uptake curves described in equation (1) assuming different values of D were also plotted in Fig. 6b to show the agreement between experiment and theoretical analysis.

Effect of water absorption and temperature on polymer chemistry

Figure 7 shows the FTIR spectra of samples before and after immersion in water at 80°C for 18 days. The bands at 1100, 1150, and 1715 cm^{-1} observed in the spectra of both coatings before immersion are assigned to C–O–C, C–O, and C=O bonds, respectively.[48] Other bands at 2853, 2925, and 2953 cm^{-1} were identified as C–H and H–C–H stretching bands.[49] The broad band at ca. 3330 cm^{-1} was the stretching band of O–H due to absorbed water molecules. More details about the

chemistry of the polymer are out of the scope of this study. After immersion in water at 80°C for 18 days, the spectra of both coatings are similar to those before immersion. This indicates that there was an insignificant change in the polymer chemistry after water immersion.

Figure 8 shows the ATR-FTIR spectra of the bisphenol A and the Novolac coatings at temperatures from 20 to 80°C. At elevated temperatures, the spectra of each coating had similar features to the one obtained from the same coating at 20°C (Fig. 8). For example, all of the characteristic bands of bisphenol A at 40, 50, 60, 70, and 80°C were at the same positions as those of the coating at 20°C. This indicates that temperature has insignificant effects on the chemistry of the coatings during short-term exposure to heat sources. A uniform increase in the intensity of the FTIR signals over the entire spectrum as the temper-
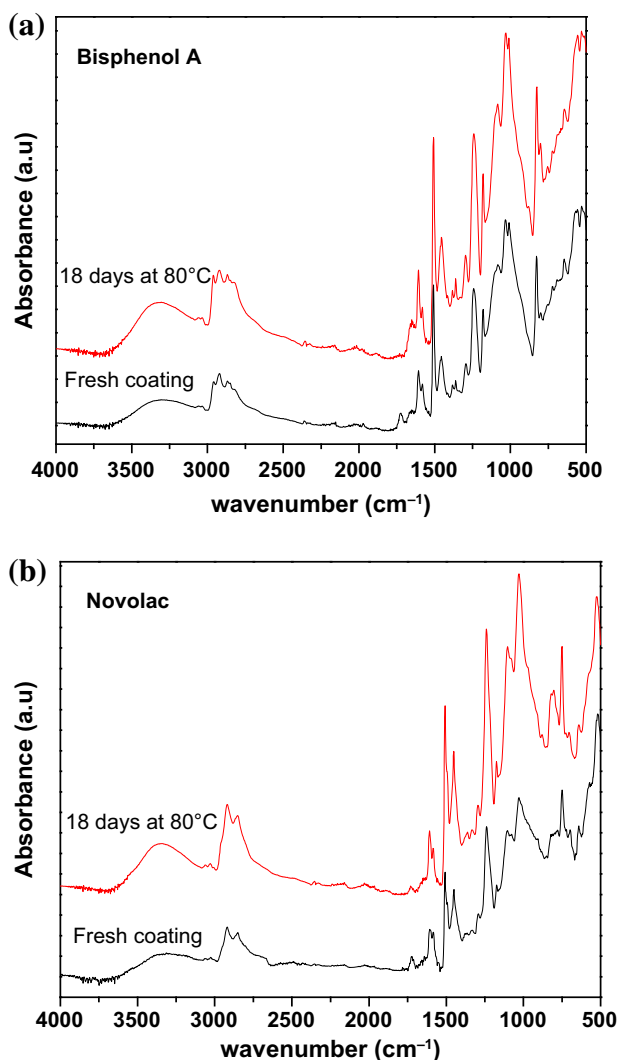
Fig. 7: FTIR spectra of the (a) bisphenol A and (b) Novolac coatings before and after immersion in water at 80°C for 18 days. The spectra were recorded at room temperature using an ATR-FTIR
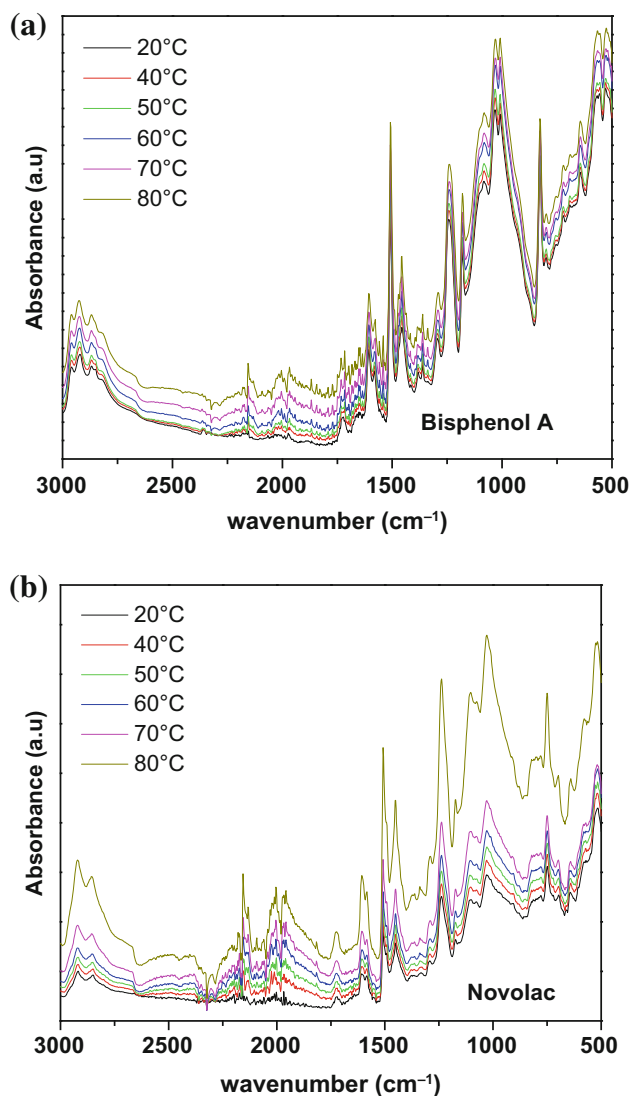
Fig. 8: FTIR spectra of the (a) bisphenol A and (b) Novolac coatings at different temperatures from 20 to 80°C. The spectra were obtained using an ATR-FTIR equipped with a temperature-controlled hot stage

ature increases is observed in Fig. 8. It is unlikely that changes in the dipole moment of the functional groups at elevated temperatures would cause this uniform signal increase because such dipole moment changes are frequency dependent.[50] Therefore, this uniform signal increase is attributed to an increase in the contact area between the samples and the ATR crystal as a result of the material deformation at elevated temperatures.

Effect of temperature on coating resistance and capacitance

Substrate-free coating films in 3 wt% NaCl solution

Bode plots of the EIS spectra of bisphenol A and Novolac coatings in 3 wt% NaCl solution at temper-

atures from 20 to 80°C are presented in Figs. 9 and 10, respectively. At 20°C, both coatings exhibited capacitance behavior dominating all frequencies from 10 mHz to 100 kHz as indicated by the 45° slope in the log Z vs log f plot and the phase angle of near −90°. The resistances of the coatings obtained by fitting the data to the equivalent circuit in Fig. 2a were in the order of 1 TΩ-cm^2. The capacitances of the coatings determined by fitting were in the order of 10^{-11} F/cm^2. The high ohmic resistance and low capacitance indicate the good corrosion protection performance of both coatings.

When the temperature increased, the impedance of both coatings decreased (Figs. 9 and 10). A plateau was observed in the impedance vs frequency plot of both coatings at temperatures above 30°C. In addition,
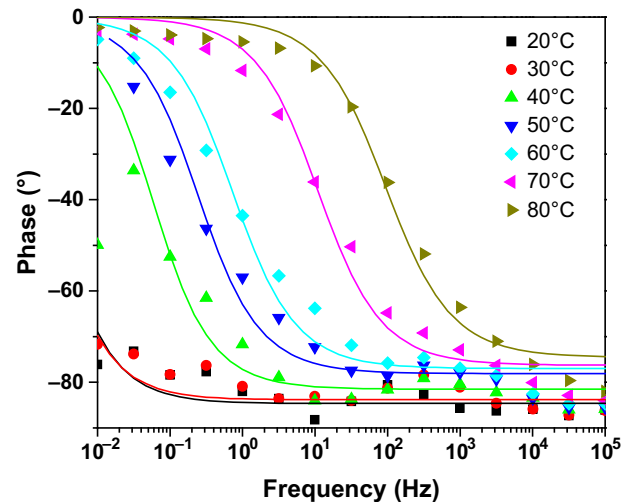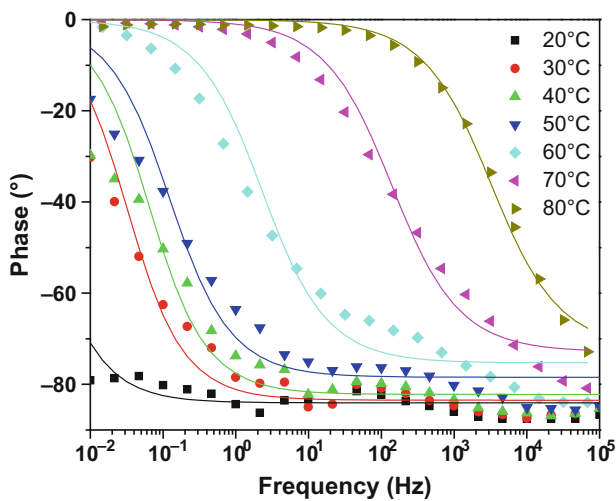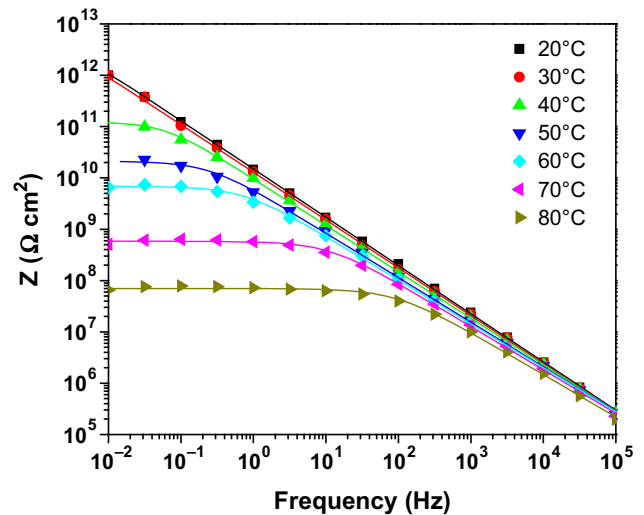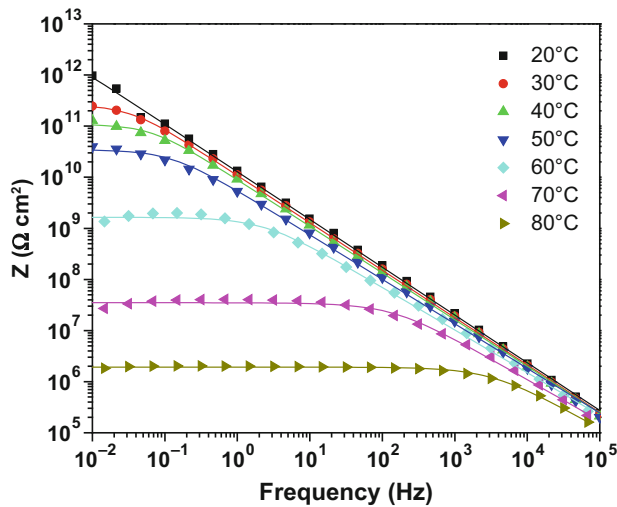
Fig. 9: Bode plot of EIS measurements on the substrate-free bisphenol A coating in 3 wt% NaCl solution using the experiment setup in Fig. 1a. The temperature of the sample was increased from 20 to 80°C and was allowed to stabilize for approximately 1 h before each EIS measurement. Experimental results are plotted in symbols and fitting results using the equivalent circuit in Fig. 2a are plotted in solid lines

Fig. 10: Bode plot of EIS measurements on the substrate-free Novolac coating in 3 wt% NaCl solution using the experiment setup in Fig. 1a. The temperature of the sample was increased from 20 to 80°C and was allowed to stabilize for approximately 1 h before each EIS measurement. Experimental results are plotted in symbols and fitting results using the equivalent circuit in Fig. 2a are plotted in solid lines

the plateau impedance decreased dramatically as the temperature increased. At 80°C, the impedance of the bisphenol A coating was 2 MΩ-cm² and the impedance of the Novolac coating was 70 MΩ-cm². A shift in the break point frequency to the high-frequency range when the temperature increased was also observed in Figs. 9 and 10. The change in the impedance and the break point frequency as temperature increased is similar to the behavior of the coating as more defects are introduced, as shown in Fig. 3.

Pore resistances and coating capacitances of the coatings at different temperatures were determined by fitting the EIS data to the equivalent circuit in Fig. 2a using an automated least square regression analysis

procedure. The EIS fitting results are plotted in solid lines in Figs. 9 and 10 along with experimental data showing good fit. The pore resistances and coating capacitances of the substrate-free coatings are plotted in Fig. 11. The pore resistance decreased exponentially when temperature increased. At 80°C, the pore resistance of bisphenol A and Novolac coatings decreased by 6 and 4 orders of magnitude, respectively, compared to the pore resistance of the same coating at 20°C (Fig. 11a). In contrast, the coating capacitances of both bisphenol A and Novolac coatings increased 6 and 12 times, respectively, when the temperature increased from 20 to 80°C (Fig. 11b). No sudden change in either
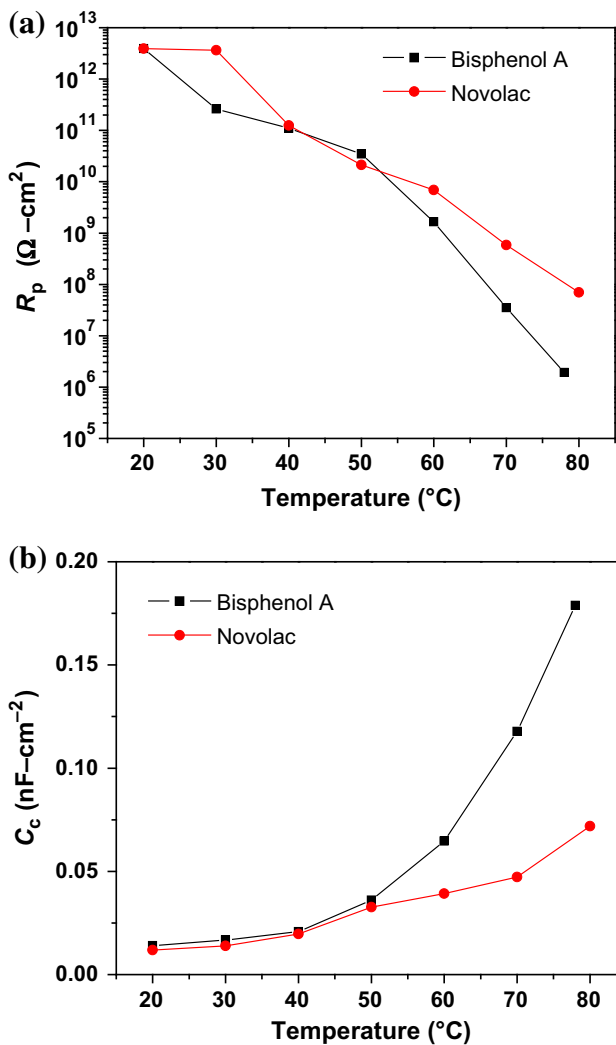
Fig. 11: Dependence of pore resistances and coating capacitances of the bisphenol A and Novolac coatings on temperature. The values were determined by fitting the EIS results to the equivalent circuit in Fig. 2a. (a) pore resistance vs temperature and (b) coating capacitance vs temperature

R_p or C_c was observed around the dry and wet glass transition temperatures of the two coatings.

Coated carbon steel in 3 wt% NaCl solution

Bode plots of the EIS spectra of bisphenol A and Novolac coatings on steel substrates in 3 wt% NaCl solution are presented in Figs. 12 and 13, respectively. At 20°C, both coated steel samples exhibited similar behavior to substrate-free films. Capacitance behavior dominated the spectra at all frequencies from 10 mHz to 100 kHz as indicated by the 45° slope in the log Z vs log f plot and the phase angle of near −90°. The coating impedance at 10 mHz and the capacitances of
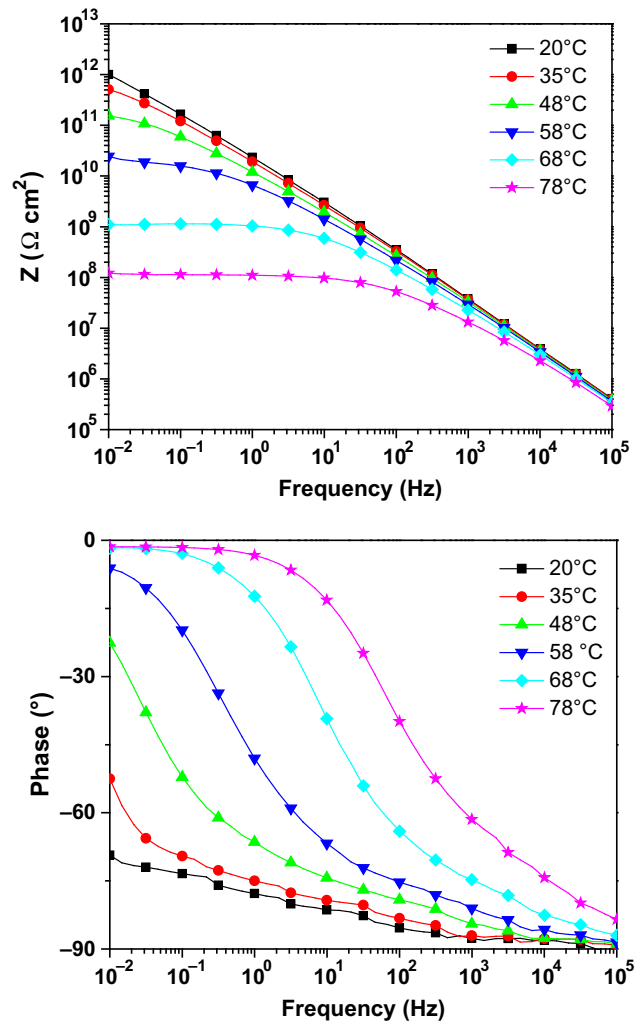
Fig. 12: Bode plot of EIS measurements on the bisphenol A-coated steel sample in 3 wt% NaCl solution using experiment setup in Fig. 1b. The temperature of the sample was increased from 20 to 80°C and was allowed to stabilize for approximately 1 h before each EIS measurement

the coatings were in the order of 1 TΩ-cm^2 and 10^{-11} F/cm^2, respectively.

When the temperature increased, the impedance of both coatings decreased (Figs. 12a and 13a). A plateau is observed in the impedance vs frequency plot of both coatings at temperatures above 50°C. In addition, the plateau impedance decreased dramatically as the temperature increased; however, it remained above 100 MΩ-cm^2 at 80°C. A shift in the break point frequency to the high-frequency range when the temperature increased was also observed in Figs. 12b and 13b.

Fitting the EIS results to the equivalent circuit in Fig. 2b resulted in a high level of uncertainty in the fitting parameters. Therefore, the coating impedances at 10 mHz were used to compare with the behavior of the substrate-free films (Fig. 14). The plot shows the

Fig. 14: Dependence of the coated steel's impedance at 10 mHz on temperature. The EIS measurements were performed in 3 wt% NaCl solution
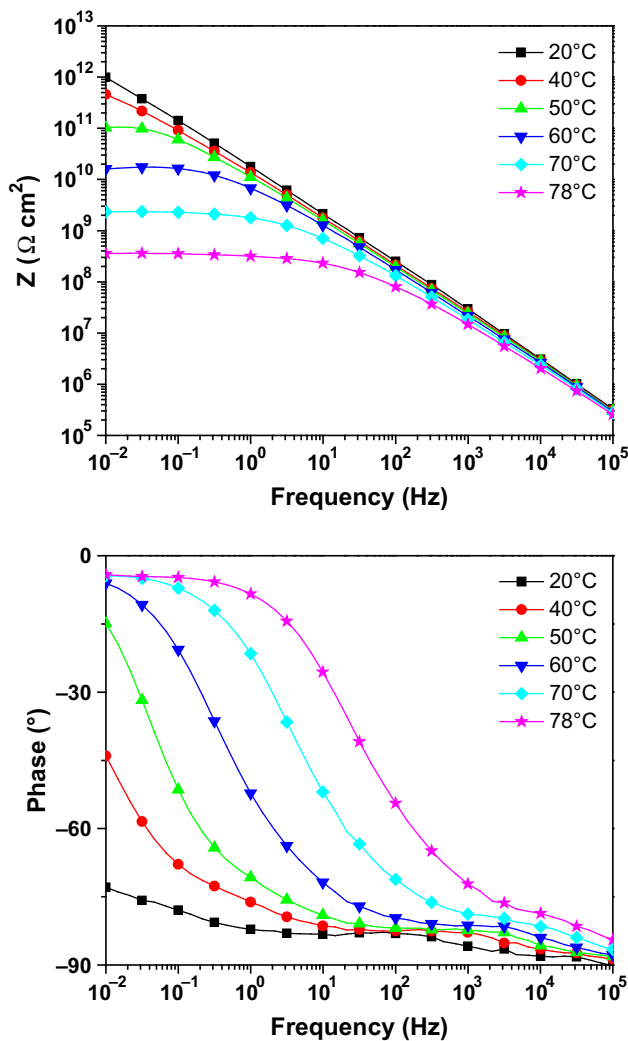

Fig. 13: Bode plot of EIS measurements on the Novolac-coated steel sample in 3 wt% NaCl solution using experiment setup in Fig. 1b. The temperature of the sample was increased from 20 to 80°C and was allowed to stabilize for approximately 1 h before each EIS measurement

deviation of the impedance–temperature relationship from the Arrhenius behavior. The impedances of the coated steel samples decreased approximately 4 orders of magnitude when the temperature increased from 20 to 80°C. At the same temperature, the impedance of the coated samples was several times higher than the impedance of the substrate-free films. For instance, the impedance of the bisphenol A-coated steel sample at 80°C was 100 MΩ-cm^2, compared to 2 MΩ-cm^2 of the bisphenol A free film at the same temperature. The difference in the extent of the impedance decrease upon rising temperature between substrate-free films and coated steel samples is associated with the difference in the level of defects created in the free films and the coated samples, which will be discussed in more detail later.
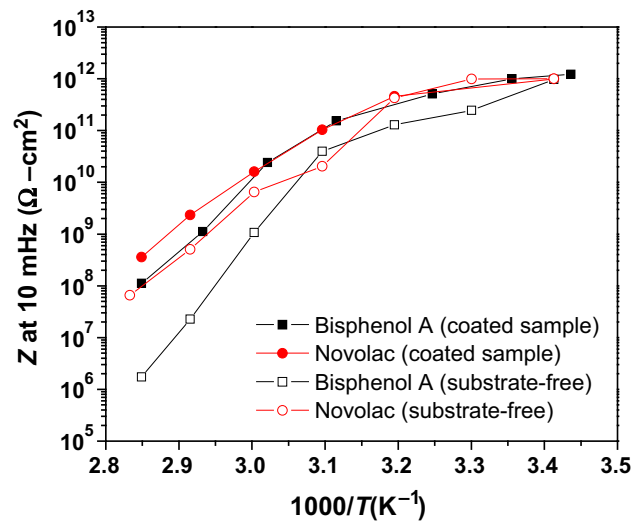
Coated carbon steel in RTIL

Bode plots of the EIS spectra of coated steel samples in ionic liquid are presented in Figs. 15 and 16, respectively. At 20°C, the spectra of both coatings in RTIL were similar to those in 3 wt% NaCl. However, at elevated temperatures, the impedances of the coatings in RTIL decreased slower than those in 3 wt% NaCl. Figure 17 shows the coating impedance at 10 mHz in RTIL and in 3 wt% NaCl solution at different temperatures. For instance, the impedance at 10 mHz of bisphenol A-coated sample in 3 wt% NaCl at 78°C decreased to 100 MΩ-cm^2 while the impedance at 10 mHz of the same coating in RTIL at 75°C was 7 GΩ-cm^2. In addition, the break point frequencies in RTIL also increased slower than in 3 wt% NaCl. The break point frequency of bisphenol A-coated sample in 3 wt% NaCl at 78°C was ca. 200 Hz compared to 6 Hz in RTIL. This marked difference in the coating behavior tested in 3 wt% NaCl and in RTIL indicates the effect of the nature of the electrolyte in the EIS measurement of polymer coatings. The worst performance of the coatings in 3 wt% NaCl solution was associated with the plasticization of the polymer upon contact with water.

Effect of repeated heating and cooling on coating performance

The pore resistance of bisphenol A- and Novolac-coating films in consecutive heating and cooling cycles in 3 wt% NaCl solution was determined by fitting the EIS spectra to the equivalent circuit in Fig. 2a. Only the data measured during rising temperature are shown in Fig. 18. Both coatings exhibited similar behavior
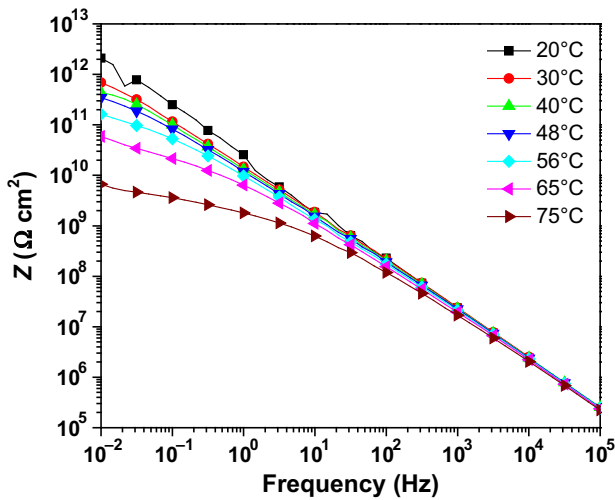
Fig. 15: Bode plot of EIS measurements on the bisphenol A-coated steel sample in room temperature ionic liquid using experiment setup in Fig. 1b. The temperature of the sample was increased from 20 to 80°C and was allowed to stabilize for approximately 1 h before each EIS measurement
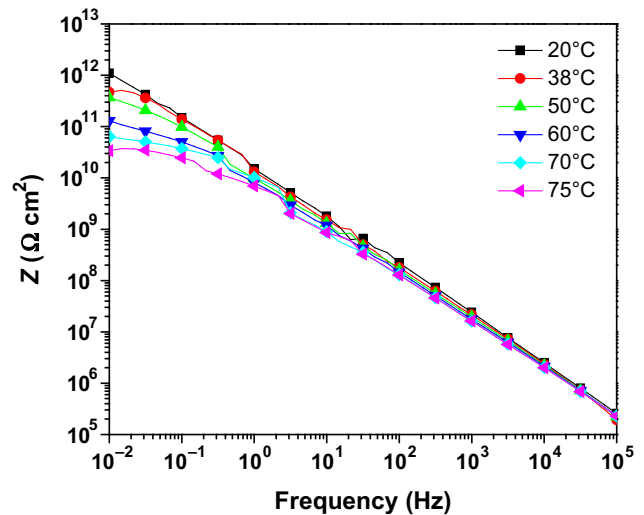

Fig. 16: Bode plot of EIS measurements on the Novolac-coated steel sample in ionic liquid using experiment setup in Fig. 1b. The temperature of the sample was increased from 20 to 80°C and was allowed to stabilize for approximately 1 h before each EIS measurement

upon repeated heating and cooling. In the first cycle, when the temperature increased from 20 to 80°C, the pore resistances of the coatings dramatically decreased by more than 4 orders of magnitude at the end of the heating cycle. After cooling down to the room temperature, the pore resistances increased to ca. 10 GΩ-cm^2, which was 2 orders of magnitude smaller than the initial pore resistance of the coatings at the beginning of the first heating cycle. In the second heating cycle, the pore resistance of both bisphenol A and Novolac decreased slower than in the first cycle and reached similar values, as in the first cycle at 80°C. The dependence of the pore resistance of the coatings on temperature in the third cycle traced that in the second cycle.

The impedances at 10 mHz of coated steel samples in 3 wt% NaCl solution in three consecutive heating/cooling cycles are shown in Fig. 19. In the first cycle, when the temperature increased from 20 to 80°C, the pore resistances of the coatings dramatically decreased by 4 orders of magnitude from ca. 1 TΩ-cm^2 at the beginning of the cycle to 100 MΩ-cm^2 at the end of the cycle. However, after cooling down to room temperature, the impedance of the coated steel samples increased to 100 GΩ-cm^2, which was 10 times higher than the impedance of the substrate-free films. In the second heating cycle, the impedance decreased in the same manner as in the first heating cycle. Similar behavior was observed in the third cycle. A shift of about 1 order of magnitude to the lower impedance was observed in the impedance vs temperature curves
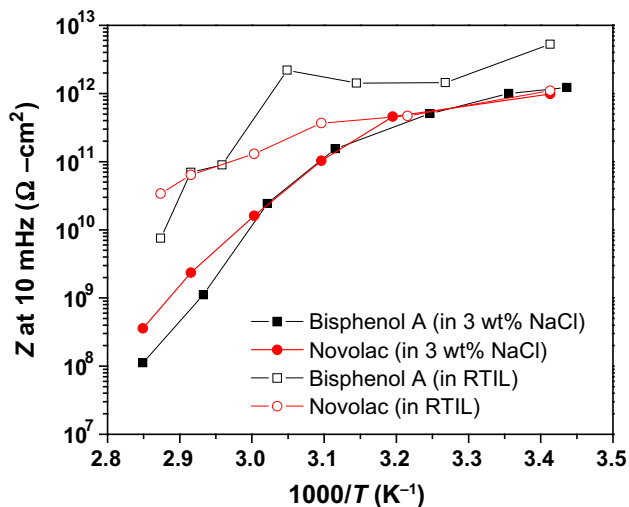
Fig. 17: Dependence of the coated steel's impedance at 10 mHz on temperature. The EIS measurements were performed in RTIL
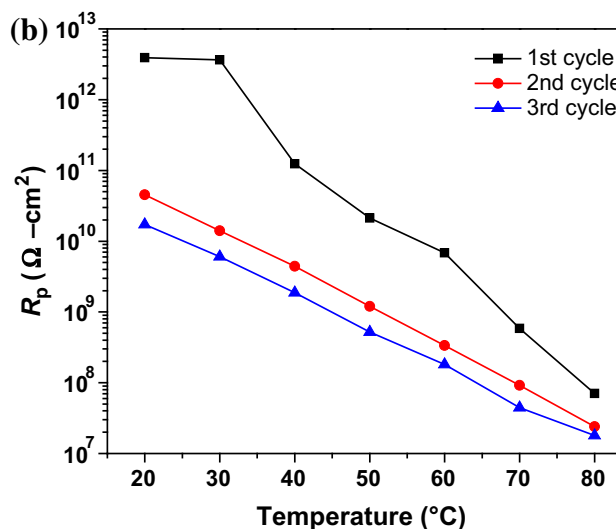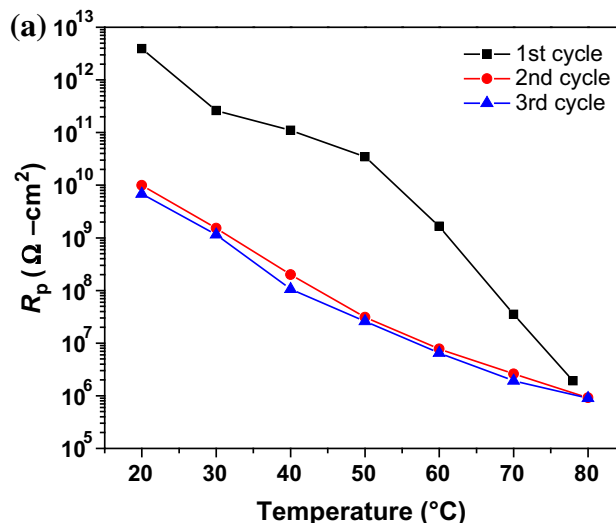

Fig. 18: Dependence of the pore resistance of (a) bisphenol A and (b) Novolac on temperature in 3 consecutive heating cycles. The pore resistances were determined by fitting the EIS spectra of the free films in 3 wt% NaCl to the equivalent circuit in Fig. 3a

after each heating/cooling cycle. This is different from the behavior of the pore resistance of the free films in which a large shift to lower resistance occurred in the resistance vs temperature curves after the first heating cycle and only a small shift occurred between the second and the third heating cycles (Fig. 18).

The change in the impedance at 10 mHz of coated steel samples in RTIL with temperature in three consecutive heating/cooling cycles is shown in Fig. 20. The coating impedance of both bisphenol A and Novolac coatings decreased approximately 3 orders of magnitude as the temperature increased from 20 to 80°C in all three heating/cooling cycles. Only a small shift of the impedance vs temperature curves after each heating/cooling cycle was observed. This behavior was markedly different from the behavior of the coatings in 3 wt% NaCl solution in which the impedance vs temperature curves were shifted several orders of magnitude after repeated heating/cooling.

Discussion

The operation temperature of pipelines is an important parameter that may dramatically change the performance of polymer coatings. Temperature may have significant effects on the structure and chemistry of polymers.[1,2] The coatings in this study experience glass transition at temperatures from 42 to 80°C, depending on the hygrothermal aging condition (Fig. 4). Chemical analysis by ATR-FTIR did not reveal any chemical change in the polymers when heated from 20 to 80°C. However, EIS results indicated that the pore resistance and the impedance of the coatings dramatically decreased when temperature increased. In addition, the coating capacitances also increased with tempera-

ture. The decrease in the coating impedance and the increase in the coating capacitance were indicative of coating degradation and the reduction of corrosion protection performance.

The decrease in the pore resistance with increasing temperature (Figs. 11a and 18) could be explained by either an increase in the solution conductivity inside the pore, a decrease in the tortuosity factor, or an increase in the pore area fraction, as described mathematically in equation (3). As temperature increased from 20 to 80°C, the conductivity of the NaCl solution increased about 2 times,[51] which could not be accounted for the reduction in the pore resistance of more than 4 orders of magnitude. Therefore, this points to the possibility that the creation of a shorter
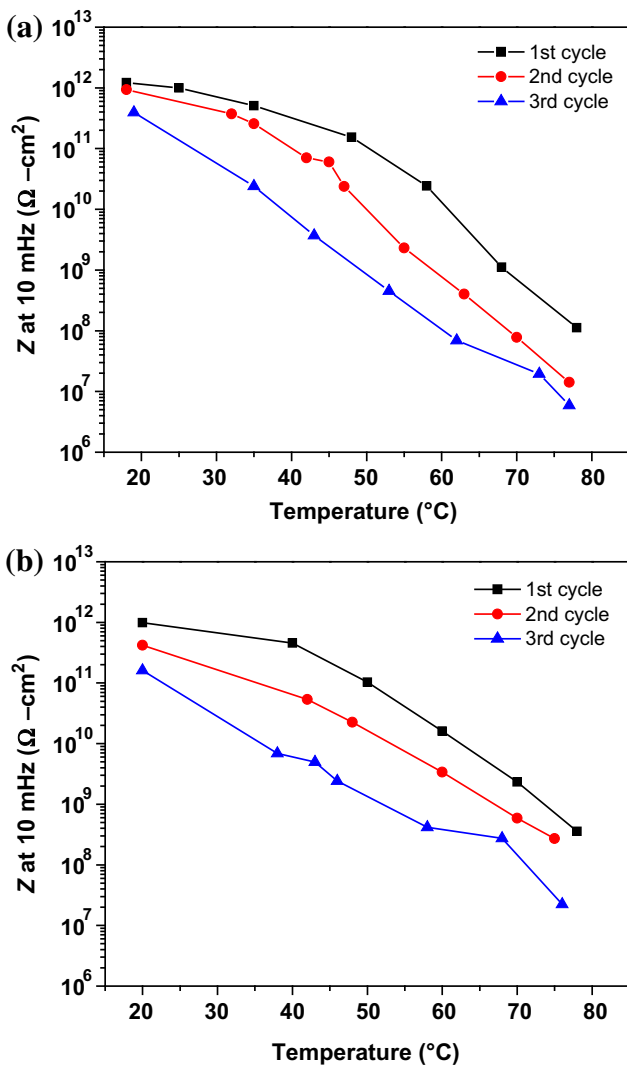
(a)

(b)

Fig. 19: Dependence of the coating impedance of the (a) bisphenol A coating and (b) Novolac coating on temperature in 3 consecutive heating cycles. The impedance was determined from EIS data of coated steel samples in 3 wt% NaCl solution using experiment setup in Fig. 1b
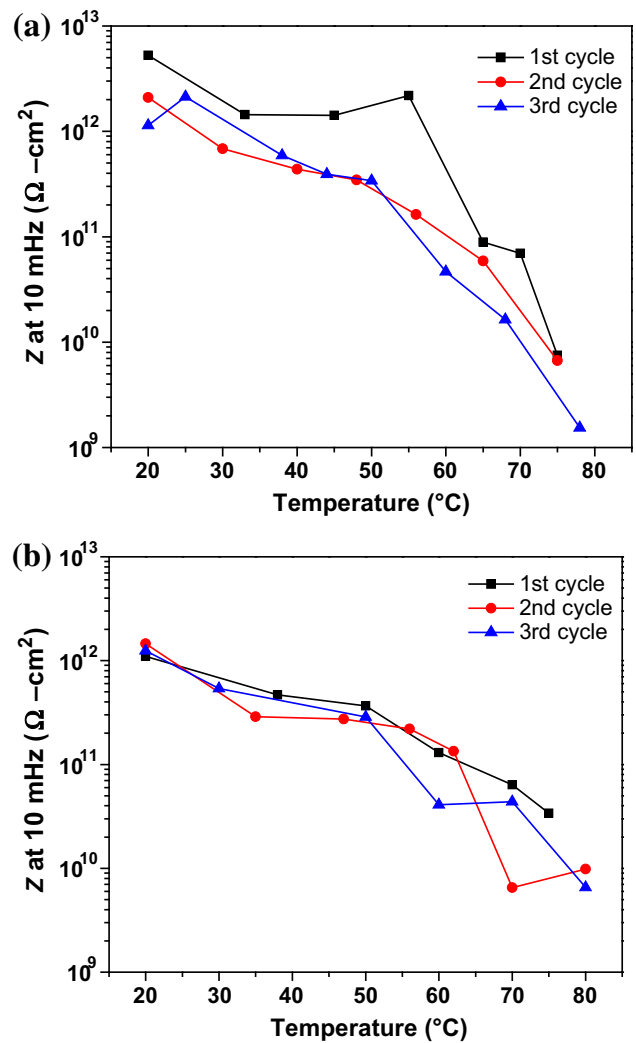
(a)

(b)

Fig. 20: Dependence of the coating impedance of the (a) bisphenol A coating and (b) Novolac coating on temperature in three consecutive heating cycles. The impedance was determined from EIS data of coated steel samples in RTIL using experiment setup in Fig. 1b

diffusion path and higher pore area fraction in the polymer during heating made a major contribution to the reduction of the pore resistance.

The pore area fraction in the coatings can be calculated from the pore resistance using the relationship in equation (8):

$$A_p = \frac{1}{\kappa} \frac{\zeta d}{R_p}. \tag{8}$$

Assume that the conductivity of the electrolyte inside pores was similar to the reported conductivity of 3 wt% NaCl solutions at the same temperature.[51] Further assume that the tortuosity of the coatings was 10 and did not change as temperature increased.

The pore area fractions of the bisphenol A and Novolac are plotted in Fig. 21. The pore fractions of both coatings at 20°C in the first cycle were in the order of 10^{-12}. At 80°C, the pore fraction of the bisphenol A coating increased to 10^{-6} and that of the Novolac coating increased to 10^{-7}. The smaller pore fraction of the Novolac coating compared to bisphenol A was in agreement with the lower water saturation level in the former compared to the latter.

The two coatings in this study exhibited a large difference in the glass transition temperatures (Fig. 4). The glass transition temperature of bisphenol A varied from 42 to 56°C and the glass transition temperature of Novolac varied from 54 to 80°C, depending on the aging condition. Nevertheless, the impedance behavior
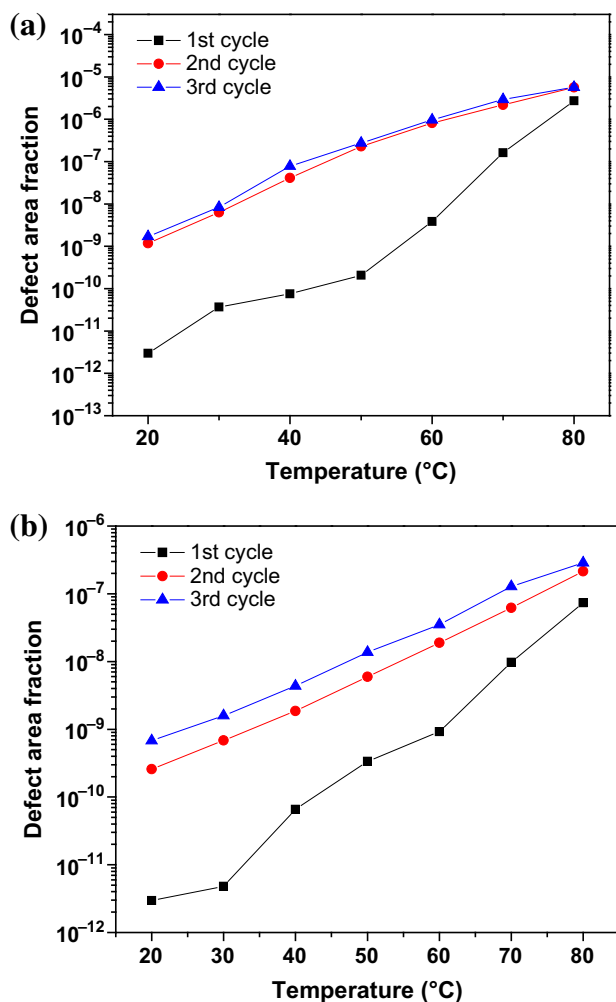
(a)

(b)

Fig. 21: Dependence of defect area fraction of (a) bisphenol A and (b) Novolac coatings on temperature. The defect area fraction was calculated using equation (8). The conductivity of the solution inside pores was assumed to be similar to the conductivity of 3 wt% NaCl corrected for temperature change. The tortuosity of the coatings was assumed to be 10 and unchanged with temperature

of both coatings was similar when the temperature was increased from 20 to 80°C. No sudden change in the coating impedance or pore fraction around the dry and wet glass transition temperatures of these coatings was observed (Figs. 18, 19, 20, and 21). Therefore, glass transition was unlikely to play an important role in decreasing the pore resistances of these coatings as the temperature increased.

The increase in the pore fraction in polymer coatings as the temperature increases could be attributed to the thermal expansion of the polymers. The increase in the volume due to thermal expansion might increase the size of the existed pores and create new pores and defects in the polymers. Moreover, the difference in the thermal expansion coefficients between different phases in the coatings might also create pores and

defects at the interfaces and interphases. This was in agreement with the increase by 2 orders of magnitude in the water diffusivity of the coatings at 80°C compared to at 20°C. When the coatings experience heating and cooling cycles, the size of the pores and defects changed according to temperature ups and downs, and therefore, the pore resistance and the overall impedance of the coatings decreased and increased, respectively (Figs. 18, 19, 20, and 21).

The decrease of T_g by 10°C in the bisphenol A coating and by 25°C in the Novolac coating after soaking in water for 3 days was associated with the plasticization effect of water on the polymer. This decrease in T_g could be explained by the interaction between absorbed water molecules and polymer molecules that disrupt the initial H bonds and Van der Waals forces between polymer chains and, hence, increase the mobility of the chains.[23,24] This water–polymer interaction created more defects and pores in the coatings that caused a larger decrease in the coating impedance when measured in 3 wt% NaCl solution (Figs. 18 and 19) compared to that in RTIL (Fig. 20). In addition, these water-induced pores were non-reversible. In repeated heating/cooling cycles, the impedance of the coatings tested in 3 wt% NaCl solution was shifted to lower values after each cycle (Figs. 18 and 19). Such shifting was not observed in RTIL (Fig. 20).

Summary

The effect of water, temperature, and glass transition on the corrosion protection behavior of two high-temperature polymer coatings for pipelines was investigated in this study. Differential scanning calorimetry (DSC) and Fourier transform infrared spectroscopy (FTIR) were used to characterize the effect of temperature and water on the structure and the chemistry of the polymer. The corrosion protection performance of the polymer was evaluated by electrochemical impedance spectroscopy. The findings are summarized as follows:

– Dried bisphenol A and Novolac coatings experienced glass transition at 52 ± 1 and 79 ± 1°C, respectively. The glass transition temperature of bisphenol A and Novolac coatings decreased to 42 ± 1 and 54 ± 1°C, respectively, after soaking in water at 20°C for 3 days but increased to 56 ± 1 and 80 ± 1°C after soaking in water at 80°C for 3 days.
– No chemical change in the polymers was detected with either dried samples or water soaked at 80°C samples when the temperature was increased from 20 to 80°C.
– Water diffusivity in bisphenol A and Novolac increased from 2.7×10^{-10} and $4.\times1 \ 10^{-10}$ cm^2/s at 20°C, respectively, to 3.0×10^{-8} and 4.1×10^{-8} cm^2/s at 80°C, respectively.

- At room temperature, both coatings exhibited good corrosion protection performance with the coating impedance in the order of 10^{12} Ω-cm^2 and the coating capacitance in the order of 10^{-11} F/cm^2.
- The pore resistance of the coatings decreased several orders of magnitude and the coating capacitance increased several times when the temperature increased from 20 to 80°C.
- During the heating and cooling cycles, the pore resistance decreased and increased correspondingly to temperature ups and downs.
- The pore resistance vs temperature curve measured in 3 wt% NaCl solution shifted to the lower impedance after each cycle. However, no significant shift in the curves was observed in RTIL.
- The effects of temperature on the impedance of the coatings were attributed to the change in the pore area fraction and the tortuosity factor of the coating associated with the thermal expansion of the polymer. The effects of temperature on the coating performance were reversible in heating/cooling cycles.
- The effects of water on the impedance of the coatings were attributed to the plasticization of the polymer. These effects were non-reversible in heating/cooling cycles in aqueous environments.
- The effects of the glass transition per se on the ohmic resistance of the coatings during a short period of exposure to heat source were insignificant.

References

1. McKenna, GB, "Glass Formation and Glassy Behavior." In: Allen, G (ed.) *Comprehensive Polymer Science and Supplements*, pp. 311–362. Pergamon, Amsterdam, 1989

2. Sperling, LH, *Introduction to Physical Polymer Science*. Hoboken, Wiley, 2006

3. Guermazi, V, et al., "Aging Effect on Thermal, Mechanical and Tribological Behaviour of Polymeric Coatings Used for Pipeline Application." *J. Mater. Process. Technol.*, **203** (1–3) 404–410 (2008)

4. Guermazi, N, Elleuch, K, Ayedi, HF, "The Effect of Time and Aging Temperature on Structural and Mechanical Properties of Pipeline Coating." *Mater. Des.*, **30** (6) 2006–2010 (2009)

5. ASTM, *Standard Practice for Operating Salt Spray (Fog) Apparatus*, in *ASTM B117 - 11*2003, ASTM International: 100 Barr Harbor Drive, West Conshohocken, PA, USA.

6. Miszczyk, A, Darowicki, K, "Accelerated Ageing of Organic Coating Systems by Thermal Treatment." *Corros. Sci.*, **43** (7) 1337–1343 (2001)

7. Fedrizzi, L, et al., "Assessment of Protective Properties of Organic Coatings by Thermal Cycling." *Progress Org Coat*, **48** (2–4) 271–280 (2003)

8. Bierwagen, GP, et al., "Studies of a New Accelerated Evaluation Method for Coating Corrosion Resistance—Thermal Cycling Testing." *Prog. Org. Coat.*, **39** (1) 67–78 (2000)

9. Angeles, ME, Rodriguez, F, Magana, C, "Effect of Heating on the Performance of Anticorrosive Coatings." *Pigm. Resin Technol.*, **41** (1) 42–48 (2012)

10. Bierwagen, GP, Tallman, DE, "Choice and Measurement of Crucial Aircraft Coatings System Properties." *Prog. Org. Coat.*, **41** (4) 201–216 (2001)

11. Bierwagen, G, et al., "EIS Studies of Coated Metals in Accelerated Exposure." *Prog. Org. Coat.*, **46** (2) 149–158 (2003)

12. Li, J, et al., "Thermal Transition Effects and Electrochemical Properties in Organic Coatings: Part 1—Initial Studies on Corrosion Protective Organic Coatings." *Corrosion*, **54** (10) 763–771 (1998)

13. Ochs, H, Vogelsang, J, "Effect of Temperature Cycles on Impedance Spectra of Barrier Coatings Under Immersion Conditions." *Electrochim. Acta*, **49** (17–18) 2973–2980 (2004)

14. Duval, S, et al., "Characterisation of Organic Coatings in Sour Media and Influence of Polymer Structure on Corrosion Performance." *Prog. Org. Coat.*, **39** (1) 15–22 (2000)

15. Haruyama, S, Asari, M, Tsuru, T, "Impedance Characteristics during Degradation of Coated Steel." *Corrosion Protection by Organic Coatings*. The Electrochemical Society, Pennington, 1987

16. Scully, JR, "Electrochemical Impedance of Organic-Coated Steel—Correlation of Impedance Parameters with Long-Term Coating Deterioration." *J. Electrochem. Soc.*, **136** (4) 979–990 (1989)

17. Kendig, M, Scully, J, "Basic Aspects of Electrochemical Impedance Application for the Life Prediction of Organic Coatings on Metals." *Corrosion*, **46** (1) 22–29 (1990)

18. Mansfeld, F, "Electrochemical Impedance Spectroscopy (Eis) as a New Tool for Investigating Methods of Corrosion Protection." *Electrochim. Acta*, **35** (10) 1533–1544 (1990)

19. Hack, HP, Scully, JR, "Defect Area Determination of Organic Coated Steels in Seawater Using the Breakpoint Frequency Method." *J. Electrochem. Soc.*, **138** (1) 33–40 (1991)

20. Murray, JN, Hack, HP, "Long-Term Testing of Epoxy-Coated Steel in ASTM Seawater Using Electrochemical Impedance Spectroscopy." *Corrosion*, **47** (6) 480–489 (1991)

21. Mansfeld, F, White, RE, "Comparing Electrochemical Impedance Spectroscopy Methods for Estimating the Degree of Delamination of Organic Coatings on Steel." *J. Electrochem. Soc.*, **140** (6) 1825 (1993)

22. van Westing, EPM, Ferrari, GM, De Wit, JHW, "The Determination of Coating Performance Using Electrochemical Impedance Spectroscopy." *Electrochim. Acta*, **39** (7) 899–910 (1994)

23. Brasher, DM, Kingsbury, AH, "Electrical Measurements in the Study of Immersed Paint Coatings On Metal. I. Comparison Between Capacitance and Gravimetric Methods of Estimating Water-Uptake." *J. Appl. Chem.*, **4** (2) 62–72 (1954)

24. Castela, AS, Simões, AM, "Assessment of Water Uptake in Coil Coatings by Capacitance Measurements." *Prog. Org. Coat.*, **46** (1) 55–61 (2003)

25. Mansfeld, F, Tsai, CH, "Discussion on the Relationship of Break-Point Frequencies to Delamination." *Corrosion*, **47** (12) 964–965 (1991)

26. Hack, H, "Defect Area Determination of Organic-Coated Steels in Seawater Using the Breakpoint Frequency Method—Reply." *J. Electrochem. Soc.*, **139** (2) 639–640 (1992)

27. Mansfeld, F, "Use of Electrochemical Impedance Spectroscopy for the Study of Corrosion Protection by Polymer Coatings—Reply." *J. Appl. Electrochem.*, **25** (12) 1145 (1995)

28. Scully, JR, Hensley, ST, "Lifetime Prediction for Organic Coatings on Steel and a Magnesium Alloy Using Electrochemical Impedance Methods." *Corrosion*, **50** (9) 705–716 (1994)

29. Hinderliter, BR, et al., "Thermal Cycling of Epoxy Coatings Using Room Temperature Ionic Liquids." *J. Electrochem. Soc.*, **155** (3) C93–C100 (2008)

30. Upadhyay, V, et al., "Preliminary Investigation of the Impact of Polymer Composition on Electrochemical Properties of Coatings as Determined by Electrochemical Impedance Spectroscopy." *J. Coat. Technol. Res.*, **10** (6) 865–878 (2013)

31. Simões, AM, Tallman, DE, Bierwagen, GP, "Use of Ionic Liquids for the Electrochemical Characterization of Water Transport in Organic Coatings." *Electrochem. Solid-State Lett.*, **8** (10) B60–B63 (2005)

32. International, A., *ASTM E2602 - 09 Standard Test Method for the Assignment of the Glass Transition Temperature by Modulated Temperature Differential Scanning Calorimetry*, 2009, ASTM International: West Conshohocken, PA.

33. Thomas, NL, "The Barrier Properties of Paint Coatings." *Prog. Org. Coat.*, **19** (2) 101–121 (1991)

34. Crank, J, *The Mathematics of Diffusion*, 2nd ed. Clarendon Press, Oxford, 1975

35. Grundmeier, G, Schmidt, W, Stratmann, M, "Corrosion Protection by Organic Coatings: Electrochemical Mechanism and Novel Methods of Investigation." *Electrochim. Acta*, **45** (15–16) 2515–2533 (2000)

36. Granata, RD, Kovaleski, KJ, "Evaluation of High-Performance Protective Coatings by Electrochemical Impedance and Chronoamperometry." *Electrochem. Impedence*, **1188** 450–462 (1993)

37. Tait, WS, et al., "Analyzing and Interpreting Electrochemical Impedance Spectroscopy Data from Internally Coated Steel Aerosol Containers." *Electrochem. Impedence*, **1188** 428–437 (1993)

38. Oliveira, CG, Ferreira, MGS, "Ranking High-Quality Paint Systems Using EIS. Part 1: Intact Coatings." *Corros. Sci.*, **45** (1) 123–138 (2003)

39. Oliveira, CG, Ferreira, MGS, "Ranking High-Quality Paint Systems Using EIS. Part II: Defective Coatings." *Corros. Sci.*, **45** (1) 139–147 (2003)

40. Choi, S, Douglas, EP, "Complex Hygrothermal Effects on the Glass Transition of an Epoxy-Amine Thermoset." *ACS Appl. Mater. Interfaces*, **2** (3) 934–941 (2010)

41. Taylor, LS, Langkilde, FW, Zografi, G, "Fourier Transform Raman Spectroscopic Study of the Interaction of Water Vapor with Amorphous Polymers." *J. Pharm. Sci.*, **90** (7) 888–901 (2001)

42. Myllytie, P, et al., "Viscoelasticity and Water Plasticization of Polymer-Cellulose Composite Films and Paper Sheets." *Cellulose*, **17** (2) 375–385 (2010)

43. Kelley, FN, Bueche, F, "Viscosity and Glass Temperature Relations for Polymer-Diluent systems." *J. Polym. Sci.*, **50** (154) 549–556 (1961)

44. Zhou, J, Lucas, JP, "Hygrothermal Effects of Epoxy Resin. Part I: The Nature of Water in Epoxy." *Polymer*, **40** (20) 5505–5512 (1999)

45. Zhou, J, Lucas, JP, "Hygrothermal Effects of Epoxy Resin. Part II: Variations of Glass Transition Temperature." *Polymer*, **40** (20) 5513–5522 (1999)

46. Philippe, LVS, et al., "Validation of Electrochemical Impedance Measurements for Water Sorption into Epoxy Coatings Using Gravimetry and Infra-red Spectroscopy." *Corros. Sci.*, **50** (3) 887–896 (2008)

47. Cao-Paz, A, et al., "Ingress of Water into Organic Coatings: Real-Time Monitoring of the Capacitance and Increase in Mass." *Prog. Org. Coat.*, **69** (2) 150–157 (2010)

48. Ayres, E, Vasconcelos, WL, Oréfice, RL, "Attachment of Inorganic Moieties onto Aliphatic Polyurethanes." *Mater. Res.*, **10** 119–125 (2007)

49. Gómez-Sánchez, E, et al., "ATR-FTIR Spectroscopy for the Characterisation of Magnetic Tape Materials. E-Preservation." *Sci. Sports*, **8** 2–9 (2010)

50. Es-sebbar, E-T, Benilan, Y, Farooq, A, "Temperature-Dependent Absorption Cross-Section Measurements of 1-Butene (1-C4H8) in VUV and IR." *J. Quant. Spectrosc. Radiat. Transf.*, **115** 1–12 (2013)

51. Bešter-Rogač, M, Neueder, R, Barthel, J, "Conductivity of Sodium Chloride in Water + 1,4-Dioxane Mixtures from 5 to 35°C II. Concentrated Solution." *J. Solut. Chem.*, **29** (1) 51–61 (2000)